INL/EXT-16-39970 Rev. 0

September 2016

MARMOT Phase-Field Model for the U-Si System

L. K. Aagesen
D. Schwen

INL/EXT-16-39970 Rev. 0

MARMOT Phase-Field Model for the U-Si System

L.K. Aagesen
D. Schwen

September 2016

Idaho National Laboratory
Fuel Modeling and Simulation Department
Idaho Falls, Idaho 83415

Prepared for the
U.S. Department of Energy
Office of Nuclear Energy
Under U.S. Department of Energy-Idaho Operations Office
Contract DE-AC07-99ID13727

ABSTRACT

A phase-field model for the U-Si system has been implemented in MARMOT. The free energies for the phases relevant to accident-tolerant fuel applications (U_3Si_2, USi, U_3Si, and liquid) were implemented as free energy materials within MARMOT. A new three-phase phase-field model based on the concepts of the Kim-Kim-Suzuki two-phase model was developed and implemented in the MOOSE phase-field module. Key features of this model are that two-phase interfaces are stable with respect to formation of the third phase, and that arbitrary phase free energies can be used. The model was validated using a simplified three-phase system and the U-Si system. In the U-Si system, the model correctly reproduced three-phase coexistence in a U_3Si_2-liquid-USi system at the eutectic temperature, solidification of a three-phase mixture below the eutectic temperature, and complete melting of a three-phase mixture above the eutectic temperature.

CONTENTS

FIGURES

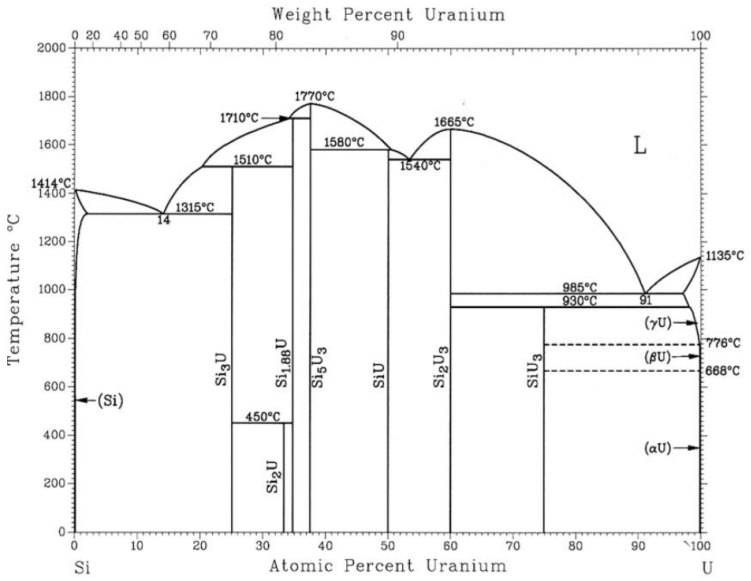

Figure 1: Phase diagram of the U-Si system [4].

1 Introduction

In recent years, the desire for commercial nuclear reactor fuels that are more tolerant of accident conditions has driven the search for alternatives to the currently used UO_2 pellets clad in zircalloy [1]. One promising candidate for accident-tolerant fuel applications is the uranium-silicon material system, which is already in use for research and test reactors [2, 3]. Si has very low solubility in the pure-U phases; similarly, U has very low solubility in diamond-cubic Si. In intermediate composition ranges, several compounds form: U_3Si, U_3Si_2, $U_{34}Si_{34.5}$ (commonly referred to as USi), U_3Si_5, $USi_{1.88}$, USi_2, and USi_3 [4]. The phase diagram of the U-Si system is shown in Fig. 1.

The U_3Si and U_3Si_2 phases have been the most closely studied for fuel applications. Although the U_3Si phase was initially more closely considered due to its higher U density, U_3Si_2 has become preferred because of its reduced swelling in-pile [5]. Compared with UO_2, U_3Si_2 has a higher uranium density and significantly higher thermal conductivity [6]. Thus, although the melting temperature of U_3Si_2 is lower than that of UO_2, the much higher thermal conductivity of U_3Si_2 results in much lower temperatures throughout the fuel pellet and greater margin to the melting temperature compared with UO_2 in both normal operation and accident scenarios.

The first step in preparation of U_3Si_2 fuel is typically arc melting of elemental U and Si. Because U_3Si_2 is a line compound, deviations from stoichiometry of the constituent U and Si and variations in processing conditions usually result in a small amounts of other phases present in the U_3Si_2 [2]. For Si-rich compositions, U_3Si_2 with embedded USi form directly from the liquid in a eutectic reaction. For Si-deficient compositions, a mixture of U_3Si_2 and body-centered cubic U with Si in solid solution is formed during solidification. A peritectoid reaction occurs below 925 °C in which solid-solution U reacts with some of the U_3Si_2 to form U_3Si. Because of kinetic limitations in this peritectoid reaction, some solid-solution U may remain following solidification, so annealing below the peritectoid temperature is typically performed following solidification to transform any remaining solid-solution U to U_3Si to stabilize the microstructure [2]. Representative U_3Si_2 microstructures with embedded USi (excess Si) and embedded U_3Si (deficient Si) are shown in Figure 2a and 2b, respectively.

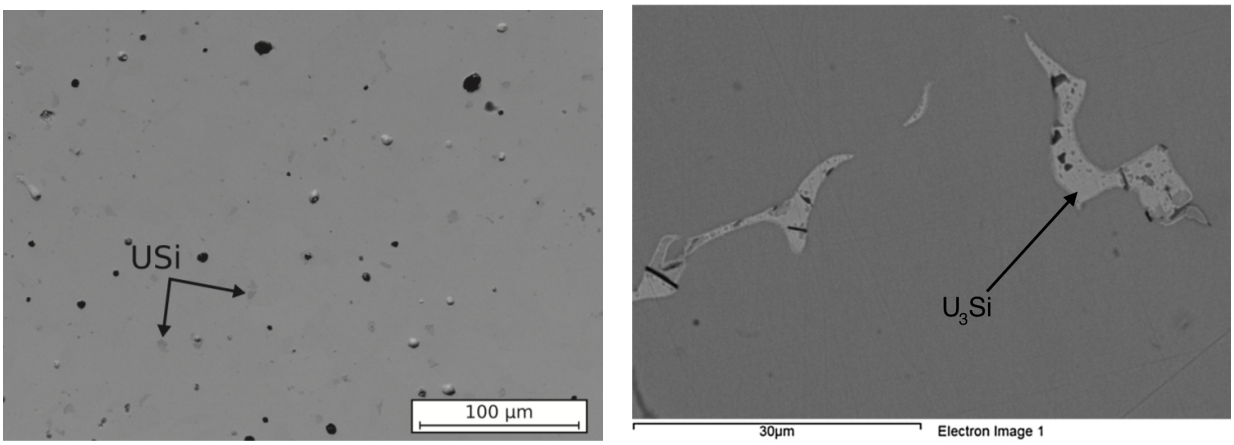

(a) (b)

Figure 2: Microstructure of U_3Si_2 with (a) excess Si [6], (b) deficient Si [7].

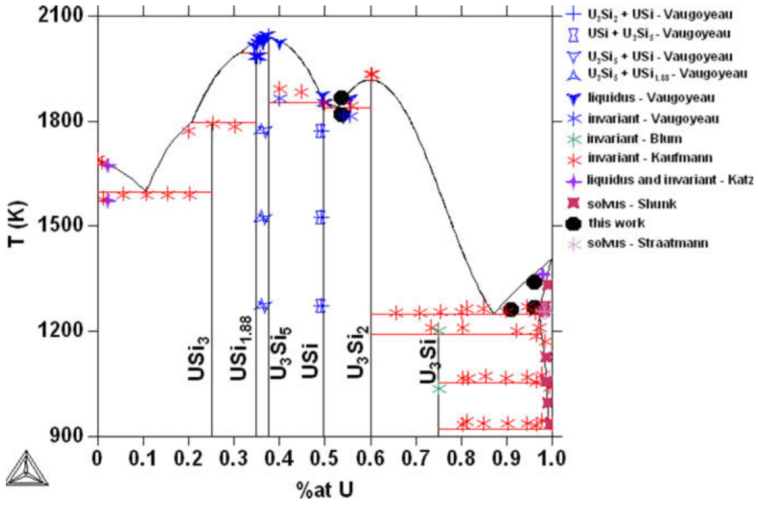

Figure 3: Calculated phase diagram of the U-Si system [8].

Berche et al. have conducted a thermodynamic study of the U-Si system [8]. They determined free energies of the phases in the system and constructed a phase diagram using these free energies using the CALPHAD method, as shown in Figure 3.

The goal of this work is to develop a phase-field model within MARMOT that will be used to investigate the evolution of microstructure in U-Si fuels during both processing and accident scenarios. The free energies determined in Ref. [8] are implemented as energy materials in MARMOT for the relevant phases, as described in Section 2. Because of the need to model liquid, U_3Si_2, and either USi or U_3Si phases simultaneously, a three-phase phase-field model based on the Kim-Kim-Suzuki (KKS) approach was developed and implemented within the MOOSE phase-field module, as described in Section 3. The advantages of this model compared to previously implemented multi-phase models are also discussed. The testing of the model with both simplified free energies and the MARMOT free energies of the U-Si system is demonstrated in Section 4. Conclusions are drawn and future applications of the model are discussed in Section 5.

2 MARMOT free energies of U-Si system

Based on a thermodynamic assessment, the free energies of the various phases in the U-Si system have been determined as a function of composition and temperature in Ref. [8]. We have implemented the free energies of the most relevant phases for fuel modeling applications (liquid, U_3Si_2, USi, and U_3Si) as free energy materials in MARMOT using the Expression Builder.

The free energy of the liquid phase is implemented in the material `USiLiqFreeEnergyMaterial` and is given by

$$\begin{aligned} G^{liq} =& c_{Si} G^{liq}_{Si} + c_U G^{liq}_U + RT\left[c_{Si}\ln c_{Si} + c_U \ln c_U\right] \\ &+ c_{Si}c_U \sum_{k=0}^{2} L^k_{(Si,U)}(c_{Si}-c_U)^k \text{J/mol} \end{aligned} \tag{1}$$

where c_{Si} and c_U are the compositions in atomic %, G^{liq}_{Si} and G^{liq}_U are the Gibbs free energies of the pure Si and U liquid phases as given by Ref. [9], R is the gas constant, T is the temperature in K, and the $L^k_{(Si,U)}$ are the temperature-dependent Redlich-Kister coefficients determined in Ref. [8]. In this and all following energy equations, the input parameters are in units of J/mol, and are converted to units of eV/nm^3 for use in simulations.

The solid phases U_3Si_2, USi, and U_3Si are line compounds, meaning that they demonstrate negligible deviation from exact stoichiometry. Thus, in Ref. [8], the free energy for each of these phases is only given at the stoichiometric composition as a function of temperature. To improve solver performance, the free energy of the solid phases has been implemented as a sharp parabola with its minimum at the energy determined for the stoichiometric phase composition and temperature determined in Ref. [8]. The free energy of the U_3Si_2 phase is implemented in the material `USiU3Si2FreeEnergyMaterial` and is

$$G^{U_3Si_2} = \frac{1}{5}\left(-171618 - 41.84T + 2G^{diamond}_{Si} + 3G^{ort}_{Si} + \frac{k}{2}(c_{Si}-0.4)^2\right) \tag{2}$$

where $G^{diamond}_{Si}$ is the Gibbs free energy of pure Si in the diamond cubic phase as given by Ref. [9], G^{ort}_U is the Gibbs free energy of pure U in the orthorhombic phase as given by Ref. [9], and k is the curvature of the parabola. The curvature of the parabolas for this and other solid phases were set to $k = 8\times10^7$ J/mol as a compromise between maintaining close to the stoichiometric composition without degrading solver performance. Sharper parabolas maintain closer to the stoichiometric composition but degrade solver performance more. Wider parabolas allow more deviation from equilibrium composition but improve solver performance. The free energy of the USi phase is implemented in the material `USiUSiFreeEnergyMaterial` and is

$$G^{USi} = \frac{1}{6.85}\left(-282080 - 34.99T + 3.45G^{diamond}_{Si} + 3.4G^{ort}_{Si} + \frac{k}{2}(c_{Si}-0.50365)^2\right) \tag{3}$$

The values for the equilibrium composition and pre-factors for the elemental phase free energies result from the fact that although this phase is normally referred to as USi, crystallographically it has been found to be $U_{34}Si_{34.5}$. The free energy of the U_3Si phase is implemented in the material `USiU3SiFreeEnergyMaterial` and is

$$G^{U_3Si} = \frac{1}{4}\left(-99727 - 11.1T + G^{diamond}_{Si} + 3G^{ort}_{Si} + \frac{k}{2}(c_{Si}-0.25)^2\right) \tag{4}$$

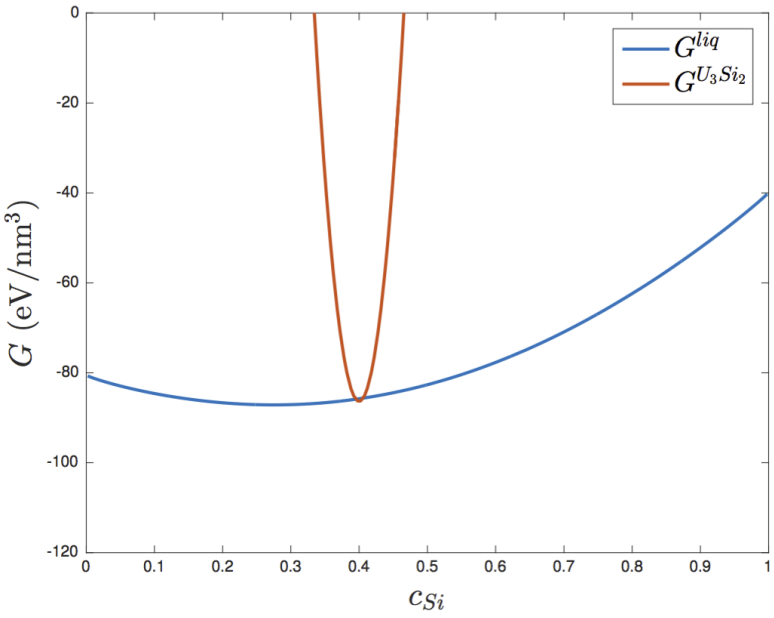

Figure 4: Plot of free energies versus c_{Si} for $T = 1813.15$ K generated using MARMOT free energy materials.

The phases initially implemented and tested were the liquid and U_3Si_2 phases. A plot of the free energies at $T = 1813.15$ K is shown in Figure 4. At this temperature, a two-phase region exists in the range of approximately $0.4 < c_{Si} < 0.48$. A common tangent exists between $c_{Si} \approx 0.4$ and $c_{Si} \approx 0.48$, so the results of the free energy plot are consistent with the published phase diagram.

To test the performance of these free energy materials in a phase-field simulation, the coexistence of a solid U_3Si_2 and liquid phase was simulated in Marmot using the original KKS two-phase phase-field model [10]. A solid-liquid interfacial energy of 0.2 J/m^2 was assumed. In the course of running these simulations, a bug in the DerivativeParsedMaterialHelper was identified that caused severe convergence problems in the solver. The bug was corrected, and convergence was dramatically improved after the bug fix. The simulation results for a steady-state two-phase simulation at $T = 1813.15$ K are shown in Figure 5.

The next phase tested was the USi phase. A plot of the free energies at $T = 1853.15$ K is shown in Figure 6. At this temperature, the liquid and USi curves are expected to cross at $c_{Si} = 0.503$, and thus the plotted results are consistent with the published phase diagram.

The coexistence of the solid U_3Si_2 and solid USi phase was simulated in Marmot using the two-phase KKS phase-field model. An interfacial energy of 1.0 J/m^2 was assumed. The simulation results for a steady-state two-phase simulation at $T = 1200$ K are shown in Figure 7. The final phase tested for fuel microstructure modeling applications was the U_3Si phase. It was tested the same manner as the other solid phases (not shown).

Before investigating three-phase microstructures, the behavior of the solid free energy materials was tested for a microstructure more representative of the actual microstructure of U_3Si_2 fuel. Because of the difficulty of maintaining exact stoichiometry between U and Si during solidification and processing, small inclusions of USi (for Si-rich conditions) or U_3Si (for Si-deficient conditions) are usually present in the U_3Si_2 matrix. An excess of approximately 0.1 wt. % Si is typically used in processing [6], which would result in 3.3 vol. % USi assuming no Si loss (this would be unlikely, but is used as an upper bound on the amount of USi present). A U_3Si_2 matrix with 3.3 vol. % U_3Si

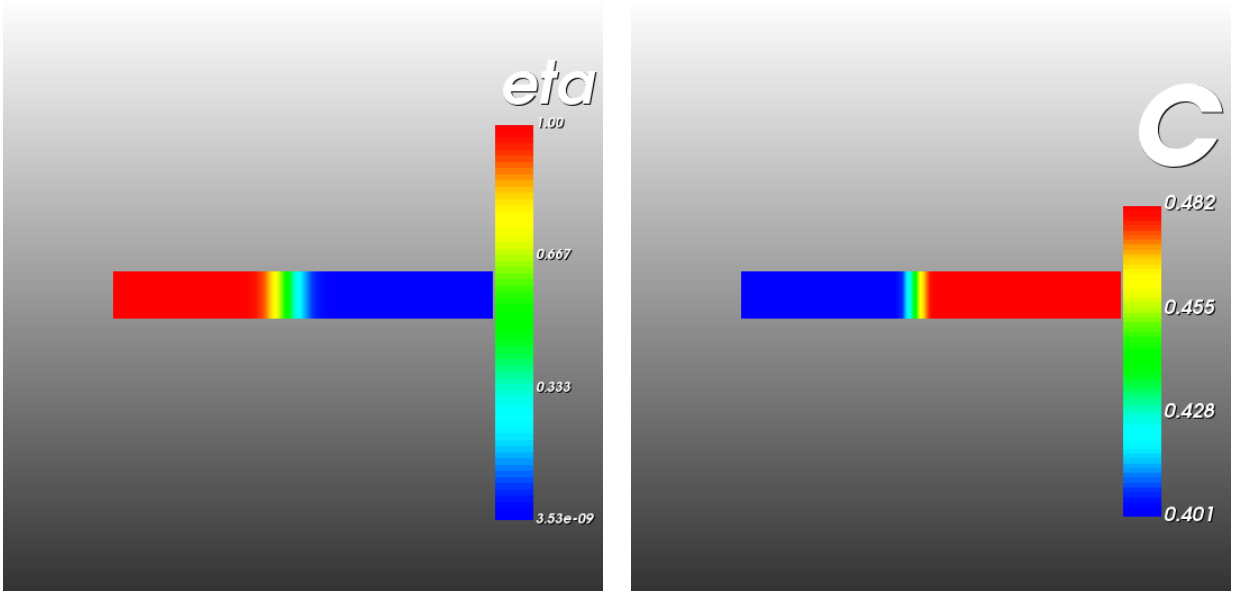

(a) η (b) c_{Si}

Figure 5: Phase-field simulation of coexistence between the solid U_3Si_2 phase and liquid phase. (a) Order parameter η representing phase of the system. $\eta = 1$ represents solid phase (left side of domain), $\eta = 0$ represents liquid phase (right side of domain). (b) Silicon concentration c_{Si} (atomic %). c_{Si} in the U_3Si_2 phase deviates slightly from the stoichiometric value of 0.4 because of the finite curvature of the parabola used to represent the line compound.

and USi was tested, as shown in Fig. 8. Solver performance was comparable to the flat interface tests.

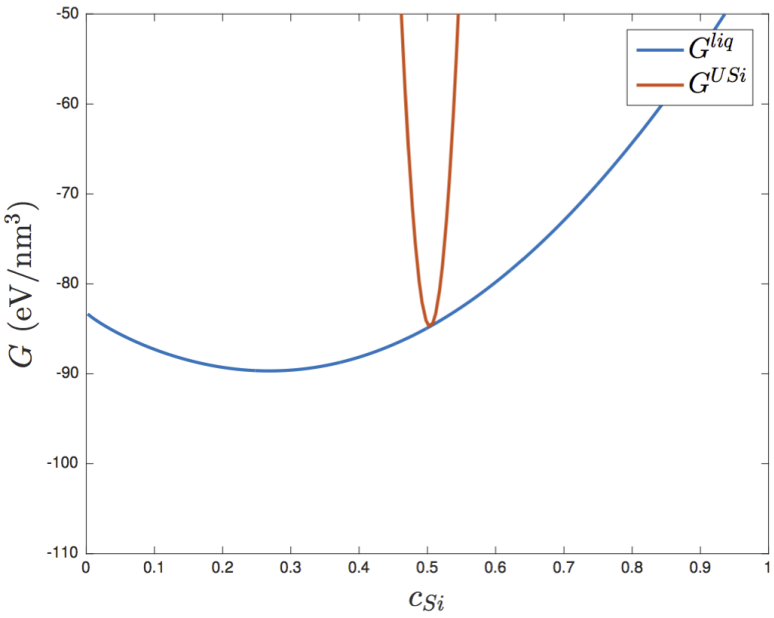

Figure 6: Plot of free energies versus c_{Si} for $T = 1853.15$ K generated using MARMOT free energy materials.

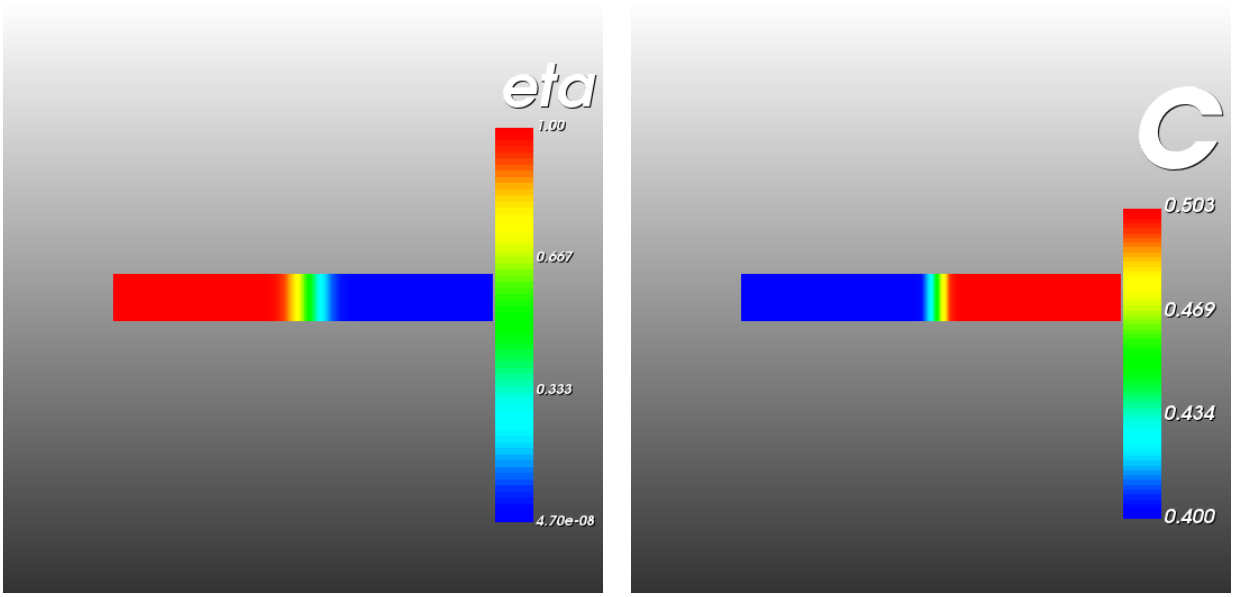

(a) η (b) c_{Si}

Figure 7: Phase-field simulation of coexistence between the solid U_3Si_2 phase and solid USi. (a) Order parameter η representing phase of the system. $\eta = 1$ represents U_3Si_2 phase (left side of domain), $\eta = 0$ represents USi phase (right side of domain). (b) Silicon concentration c_{Si} (atomic %). Deviation from stoichiometry is not observed because the minima of the free energies are close in magnitude at this temperature.

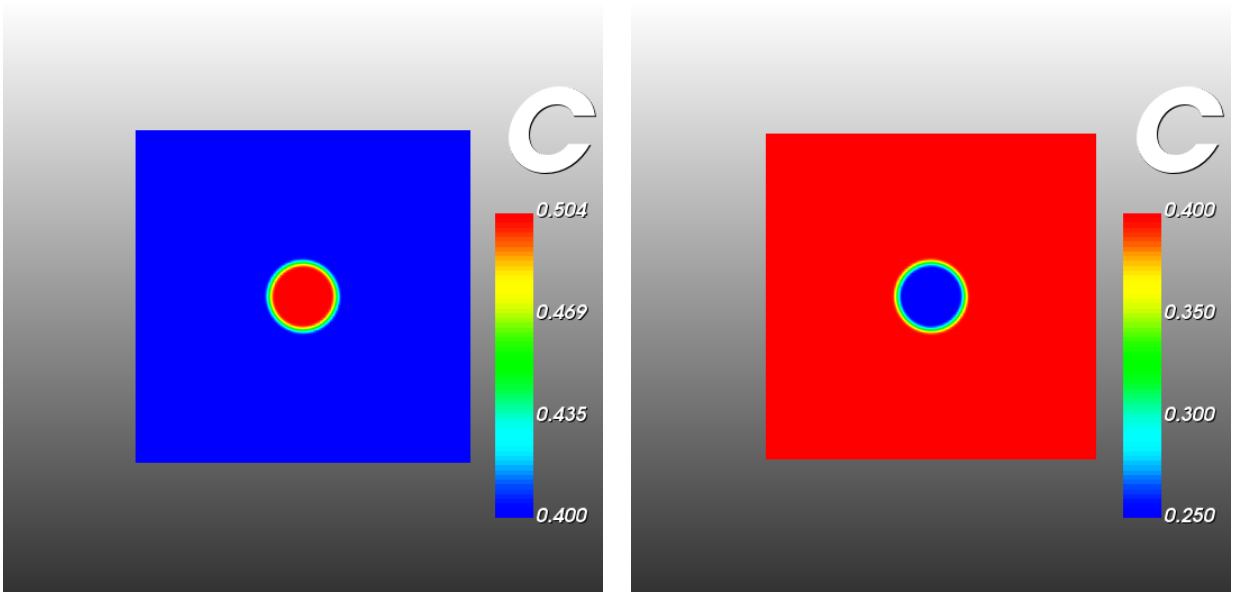

(a) USi in U_3Si_2 matrix.

(b) U_3Si in U_3Si_2 matrix

Figure 8: (a) USi precipitate (red) embedded in U_3Si_2 matrix (blue). (b) U_3Si precipitate (blue) embedded in U_3Si_2 matrix (red).

3 Three-phase KKS phase-field model

Because U_3Si_2 is a line compound, depending on variations in stoichiometry and processing, small amounts of either USi or U_3Si usually form in U_3Si_2 for fuel applications. Thus, to investigate the microstructure of U_3Si_2 during solidification processing or accident scenarios, a three-phase phase-field model is necessary to represent the liquid, U_3Si_2, and USi (or U_3Si) phases. One limitation of many previously developed multi-phase phase-field models is that a binary interface between two phases is unstable with respect to the spurious formation of additional phases in the diffuse interfacial region [11, 12]. This spurious third-phase formation distorts the interfacial energy of the binary interface and can lead to nucleation of the third phase in unphysical locations.

To avoid this spurious third-phase formation, we have implemented in the MOOSE framework a three-phase KKS model similar in approach the model described in Ref. [13]. Like the original two-phase KKS model [10], it uses an equal chemical potential condition to remove the bulk chemical contribution from the interfacial region, and decouples interfacial energy from interfacial thickness. The tilting functions developed in Ref. [11] are used to prevent spurious third-phase formation at a binary interface.

In this model, the three phases are represented by order parameters η_1, η_2, and η_3, which are constrained such that

$$\eta_1 + \eta_2 + \eta_3 = 1 \tag{5}$$

The free energy of the system is given by

$$F = \int_V \left[f_{bulk} + f_{grad} + \lambda \left(1 - \sum_i \eta_i \right) \right] dV \tag{6}$$

where λ is a Lagrange multiplier used to enforce the constraint of Eq. 5. The bulk energy f_{bulk} is given by

$$f_{bulk} = h_1(\vec{\eta}) f_1(c_1) + h_2(\vec{\eta}) f_2(c_2) + h_3(\vec{\eta}) f_3(c_3) + \sum_i W \eta_i^2 (1 - \eta_i)^2 \tag{7}$$

where f_i is the free energy of each phase, c_i is the phase composition, W is the potential barrier height, and the h_i are the tilting functions [11, 13]

$$h_i(\vec{\eta}) = h_i(\eta_i, \eta_j, \eta_k) = \frac{\eta_i^2}{4} \{ 15(1 - \eta_i)[1 + \eta_i - (\eta_k - \eta_j)^2] + \eta_i(9\eta_i^2 - 5) \} \tag{8}$$

The gradient energy f_{grad} is given by

$$f_{grad} = \sum_i \frac{\kappa}{2} |\nabla \eta_i|^2 \tag{9}$$

The composition c is defined as a function of the phase compositions as

$$c = h_1(\vec{\eta}) c_1 + h_2(\vec{\eta}) c_2 + h_3(\vec{\eta}) c_3 \tag{10}$$

Because the tilting function h_i reduces to the commonly used two-phase interpolation function $h(\eta) = \eta_i^3(10 - 15\eta_i + 6\eta_i^2)$ along the two-phase interfaces [11], this constraint on the compositions reduces to that used in the two-phase KKS model [10] for i-j interfaces:

$$c = h(\eta_i) c_i + [1 - h(\eta_i)] c_j \tag{11}$$

The phase concentrations are constrained such that the chemical potentials of each phase are equal:

$$\mu = \frac{\partial f_1}{\partial c_1} = \frac{\partial f_2}{\partial c_2} = \frac{\partial f_3}{\partial c_3} \tag{12}$$

The time evolution of the order parameters is given by the Allen-Cahn equation

$$\frac{\partial \eta_i}{\partial t} = -L \frac{\delta F}{\delta \eta_i}\bigg|_{\sum \eta_i = 1} \tag{13}$$

where t is the time, L is the Allen-Cahn mobility, and the variational derivative is evaluated considering the constraint of Equation 5. Using the fact that $\frac{\partial}{\partial t}\sum_i \eta_i = 0$ and assuming the mobilities for each phase are equal at each position (though they may be dependent on the local values of the order parameters), the Lagrange multiplier can be eliminated and the constrained variational derivative can be written in terms of the non-constrained variational derivatives as

$$\frac{\delta F}{\delta \eta_i}\bigg|_{\sum \eta_i = 1} = \frac{\delta F}{\delta \eta_i} - \frac{1}{3}\sum_j \frac{\delta F}{\delta \eta_j} \tag{14}$$

Substituting for F,

$$\frac{\partial \eta_i}{\partial t} = -L\left[\frac{2}{3}\left(\frac{\partial f_{bulk}}{\partial \eta_i} - \nabla \cdot \frac{\partial f_{grad}}{\partial \nabla \eta_i}\right) - \frac{1}{3}\left(\frac{\partial f_{bulk}}{\partial \eta_j} - \nabla \cdot \frac{\partial f_{grad}}{\partial \nabla \eta_j}\right) - \frac{1}{3}\left(\frac{\partial f_{bulk}}{\partial \eta_k} - \nabla \cdot \frac{\partial f_{grad}}{\partial \nabla \eta_k}\right)\right] \tag{15}$$

where

$$\begin{aligned}\frac{\partial f_{bulk}}{\partial \eta_i} =& \frac{\partial h_i}{\partial \eta_i}[f_i(c_i) - \mu c_i] + \frac{\partial h_j}{\partial \eta_i}[f_j(c_j) - \mu c_j] + \frac{\partial h_k}{\partial \eta_i}[f_k(c_k) - \mu c_k] \\ &+ 4W\eta_i(\eta_i - 1)(\eta_i - \frac{1}{2})\end{aligned} \tag{16}$$

and

$$\nabla \cdot \frac{\partial f_{grad}}{\partial \nabla \eta_i} = \kappa \nabla^2 \eta_i \tag{17}$$

The time evolution of the composition field is given by the Cahn-Hilliard equation:

$$\frac{\partial c}{\partial t} = \nabla \cdot \left[M_c \nabla \frac{\delta F}{\delta c}\right] \tag{18}$$

where M_c is the Cahn-Hilliard mobility. It can be shown that this is equivalent to

$$\frac{\partial c}{\partial t} = \nabla \cdot \left[D \sum_i h_i \nabla c_i\right] \tag{19}$$

where D is the solute diffusion coefficient.

4 Testing of three-phase KKS model and U-Si free energies

The three-phase KKS model was tested with both a simplified material system free energies and the U-Si system free energies described in Section 2.

4.1 Testing with simplified material system

One of the most important features of the three-phase KKS model is that the third phase will not form at the interface between the other two phases. To test this property, a simplified material system was used, consisting of two chemical species and three phases. The local composition is represented with a single composition variable c, and the three phases have equilibrium compositions of $c = 0.2, 0.5$, and 0.8. The free energy of each phase is given by

$$f = k_s(c_i - c_{i,eq})^2 \tag{20}$$

where $k_s = 20$ is the (nondimensional) curvature of the parabola, c_i is the phase composition for phase i, and $c_{i,eq}$ is the equilibrium composition of each phase; $c_{1,eq} = 0.2$, $c_{2,eq} = 0.5$, and $c_{3,eq} = 0.8$. Using this dimensionless model system, a binary, 1D interface between phase 1 and phase 3 was created and allowed to equilibrate. The analytical solution for the equilibrium shape of the order parameter η_1 through a two-phase interface is given by

$$\eta_1 = \frac{1}{2}\left[1 - \tanh\left(\frac{x - x_0}{\sqrt{2}\delta}\right)\right] \tag{21}$$

where x_0 is the midpoint of the interface and $\delta = \sqrt{\kappa/W}$ is the characteristic thickness of the interface. In equilibrium the analytical solution also predicts $\eta_2 = 0$ and $\eta_3 = 1 - \eta_1$. The analytical solution for c can be determined from Equation 10 by substituting the equilibrium order parameter profiles into the h_i and using the fact that $c_i = c_{i,eq}$ at equilibrium.

As shown in Figure 11, the equilibrium order parameter profiles and composition profile matched the analytical solutions. There was no formation of phase 2 ($\eta_2 = 0$ throughout, not shown). The stability of the binary interface is a significant advantage of the three-phase KKS formulation, because the formation of the third phase can significantly affect the interfacial energy between phases. This test was repeated with a uniform value of $\eta_2 = 0.1$ in the initial conditions to verify that the η_2 phase would disappear, which it did, leaving the η_1-η_3 interface as expected.

To verify that the three-phase KKS model would produce the correct physical behavior, a circular η_1 particle was embedded in an η_2 matrix, and the composition shift due to the Gibbs-Thomson effect in both phases was compared to the analytical solution. The Gibbs-Thomson shift in composition on either side of the interface between these phases is given by [14]

$$\Delta c = c - c_{i,eq} = \frac{H\gamma_{int}}{A(c_{2,eq} - c_{1,eq})} \tag{22}$$

where $H = \frac{1}{r}$ is the curvature of the particle-matrix interface and $r = 10$ is the particle radius, $\gamma_{int} = \frac{\sqrt{2\kappa W}}{3}$ is the interfacial energy in the phase-field model (in which currently only equal interfacial energies are implemented), and A is the second derivative of the free energy with respect to composition. Using Equation 20, and $A = 40$ for both phases, the composition shift in the simulation at equilibrium agreed with the analytical solution within 0.01%.

Before testing the more complex U-Si system, the behavior of the three-phase KKS model was also investigated for the model system for initial conditions where all three phases were present.

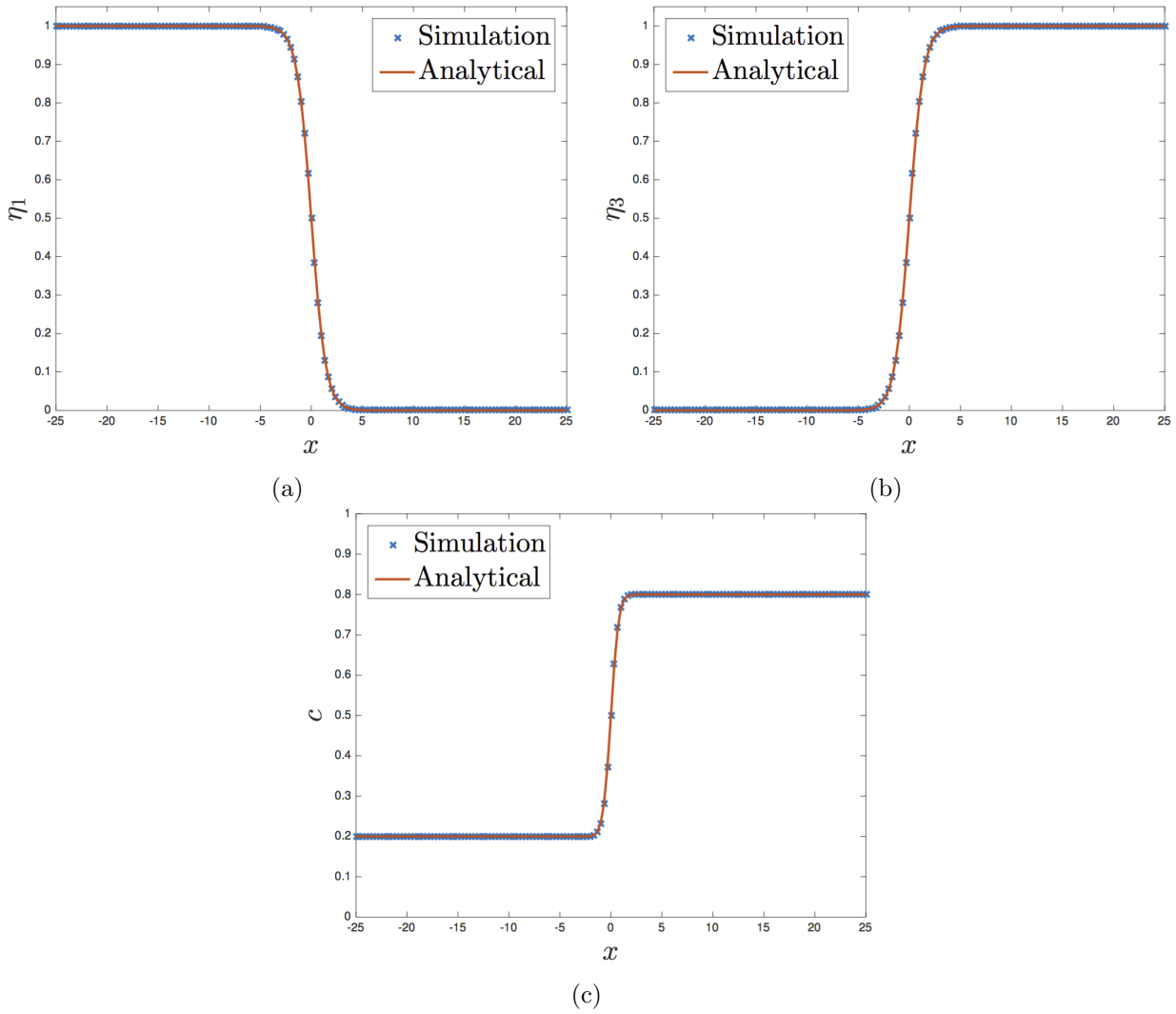

Figure 9: Interface between phase 1 and phase 3 at equilibrium for simplifed system. (a) η_1, (b) η_3, (c) composition. The order parameter field for η_2 remained zero at all times.

Since the minima for the free energy curves for each of the phases were at zero, the free energies lie on a common tangent (this is physically equivalent to a eutectic temperature). Thus, the three phases can coexist in equilibrium. This is demonstrated in Figure 10a for a tri-crystal geometry with flat interfaces and in Figure 10b for a trijunction configuration. Because the interfacial energies for the three types of interface are equal in the current implementation, the contact angles at the trijunction are expected to be equal to 120°.

4.2 Testing three-phase KKS model with U-Si free energies

Having verified that the three-phase KKS model produces the correct physical behavior for a simplified model system, the U-Si phases were tested in the three-phase model. Mixtures of liquid, U_3Si_2, and USi were initially investigated because these phases can coexist as a eutectic. In Ref. [8], the eutectic temperature was determined to be 1840 K, but the precise composition of the eutectic point was not specified. By equilibrating a two-phase liquid-U_3Si_2 system at 1840 K, the composition c_{Si}

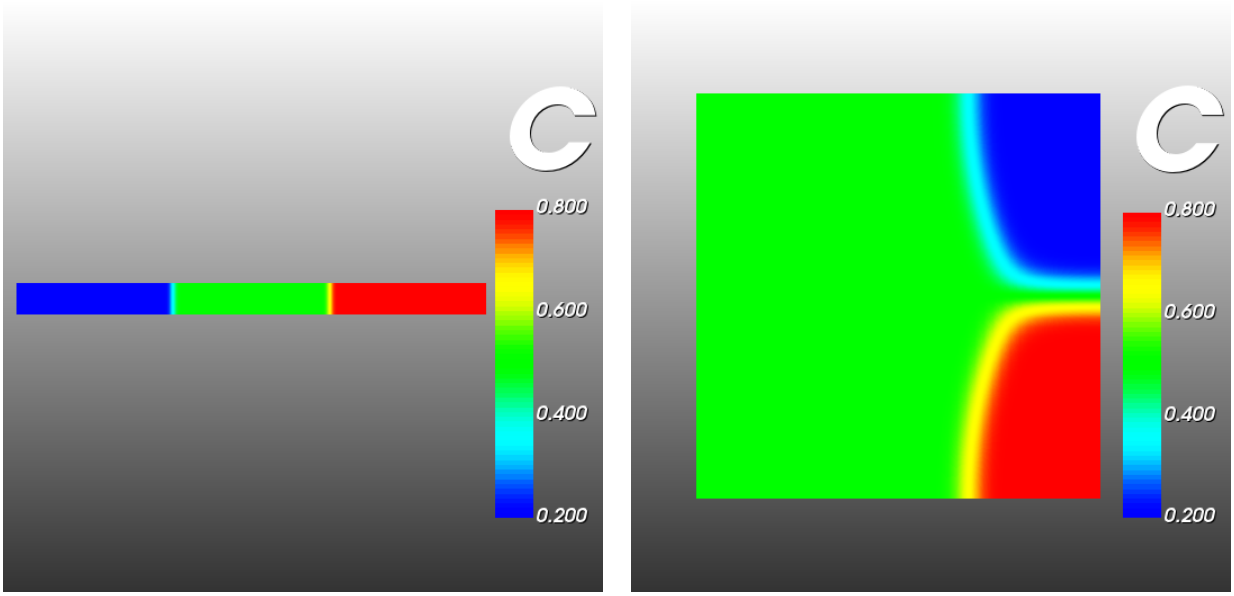

(a) (b)

Figure 10: Coexistence between phase 1, phase 2, and phase 3 at eutectic point in the three-phase KKS model. (a) tri-crystal configuration, (b) trijunction configuration. Composition $c = 0.2$ is phase 1, $c = 0.5$ is phase 2, and $c = 0.8$ is phase 3.

at the eutectic point in their assessment was determined to be 0.4711.

A simulation of the three phases at the eutectic temperature of 1840 K is shown in Figure 11a. This configuration was in equilibrium, and the compositions of the U_3Si_2 and USi phases are shifted slightly as expected because of the finite curvatures of the parabolas used to represent the free energies of these line compounds.

Having verified the correct behavior of the system at the eutectic temperature, the behavior of the system below and above the eutectic temperature was investigated. Figure 11b shows the initial conditions, a liquid U-Si region (center) between a region of U_3Si_2 (left) and USi (right). The system was at a temperature of 1800 K, which resulted in the liquid solidifying, leaving a bicrystal of U_3Si_2 (left) and USi (right), as shown in Figure 11c. The order parameter η_1 representing the liquid was zero throughout. The same initial condition in Figure 11b was then held at a temperature of 1920 K. At this temperature, the entire domain melted, as evidenced by the fact that $\eta_1 = 0$ throughout at the end of the simulation. Some inhomogeneity in composition remained as a result of the initial condition, shown in Figure 11d.

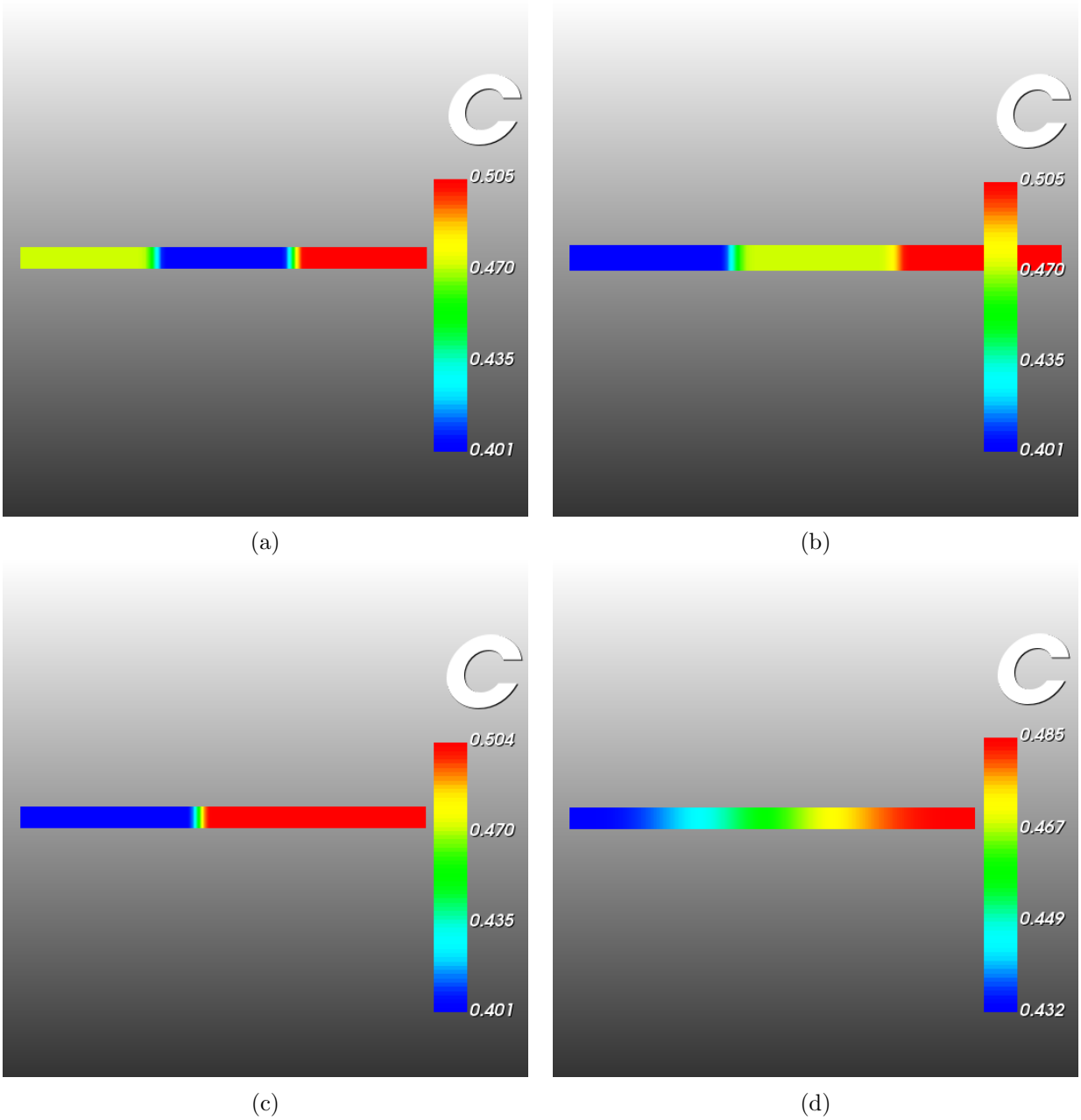

(a) (b) (c) (d)

Figure 11: Behavior of U-Si system. (a) Coexistence of liquid U-Si (left), U_3Si_2 (center), and USi (right) at eutectic temperature 1840 K. (b) Initial condition of melting/freezing simulations: U_3Si_2 (left), liquid U-Si (center), and USi (right). (c) Freezing at 1800 K: two-phase domain of U_3Si_2 (left) and USi (right) remains with no liquid remaining ($\eta_1 = 0$ throughout, not shown). (d) Melting at 1920 K: single-phase domain remains ($\eta_1 = 1$, $\eta_2 = \eta_3 = 0$ throughout, not shown).

5 Summary

To investigate the evolution of microstructure in fuels based on the U-Si materials system, a phase-field model of this system has been developed. Free energies of the phases in the system relevant to nuclear fuels (U_3Si_2, USi, U_3Si, and liquid) were implemented in MARMOT based on a on a thermodynamic assessment conducted using the CALPHAD method. To model realistic microstructures of U_3Si_2 fuel during solidification processing and accident scenarios, a three-phase KKS phase model was developed. Key features of this model are that two-phase interfaces are stable with respect to formation of the third phase, and that arbitrary phase free energies can be used. This model was tested with a simplified three-phase system and the U_3Si_2-liquid-USi system. Using the simplified system, stability of the two-phase interface was demonstrated, and it was shown that the profiles of the order parameter and composition fields through the interface matched the analytical solutions. It was also shown that the Gibbs-Thomson shift in composition on either side of the interface between a circular particle and the matrix was in agreement with the analytical solution. In the U-Si system, model correctly reproduced three-phase coexistence in a U_3Si_2-liquid-USi system at the eutectic temperature, solidification of a three-phase mixture below the eutectic temperature, and complete melting of a three-phase mixture above the eutectic temperature.

Future plans for this system include implementing unequal interfacial energies between phases. Methods to do so are described in Ref [11, 13]. This will require implementing an additional kernel in the MOOSE phase-field model. Using data from lower length scale calculations, interfacial energies in the U-Si system can be calculated and used as input to the phase-field model. Using the fully parameterized model, the behavior of U_3Si_2 fuel in accident scenarios will be investigated by imposing a temperature profile experienced in accident conditions and determining when liquid formation occurs for different microstructures.

6 References

1. Roadmap: Development of light water reactor fuels with enhanced accident tolerance. Report INL/EXT-12-25305, Idaho National Laboratory, 2012.

2. J. L. Snelgrove, R. F. Domagala, G. L. Hofman, T. C. Wiencek, G. L. Copeland, R. W. Hobbs, and R. L. Senn. The use of U3Si2 dispersed in aluminum in plate-type fuel elements for research and test reactors. Report ANL/RERTR/TM-11, Argonne National Laboratory, 1987.

3. Y.S. Kim. *Uranium Intermetallic Fuels*, volume 3, pages 391–420. Elsevier, 2012.

4. T.B. Massalski, editor. *Binary Alloy Phase Diagrams, 2nd Ed.*, pages 3374–3375. ASM, Materials Park, OH, 1990.

5. Y.S. Kim and G. L. Hofman. Interdiffusion in U3Si-Al, U3Si2-Al, and USi-Al dispersion fuels during irradiation. *Journal of Nuclear Materials*, 410(1-3):1–9, 2011.

6. J. T. White, A. T. Nelson, J. T. Dunwoody, D. D. Byler, D. J. Safarik, and K. J. McClellan. Thermophysical properties of U3Si2 to 1773 K. *Journal of Nuclear Materials*, 464:275–280, 2015.

7. J. M. Harp, P. A. Lessing, and R. E. Hoggan. Uranium silicide pellet fabrication by powder metallurgy for accident tolerant fuel evaluation and irradiation. *Journal of Nuclear Materials*, 466:728–738, 2015.

8. A. Berche, C. Rado, O. Rapaud, C. Guneau, and J. Rogez. Thermodynamic study of the U-Si system. *Journal of Nuclear Materials*, 389(1):101–107, 2009.

9. A. T. Dinsdale. SGTE data for pure elements. *Calphad-Computer Coupling of Phase Diagrams and Thermochemistry*, 15(4):317–425, 1991.

10. S. G. Kim, W. T. Kim, and T. Suzuki. Phase-field model for binary alloys. *Physical Review E*, 60(6):7186–7197, 1999.

11. R. Folch and M. Plapp. Quantitative phase-field modeling of two-phase growth. *Physical Review E*, 72(1), 2005.

12. G. I. Toth, T. Pusztai, and L. Granasy. Consistent multiphase-field theory for interface driven multidomain dynamics. *Physical Review B*, 92(18), 2015.

13. M. Ohno and K. Matsuura. Quantitative phase-field modeling for two-phase solidification process involving diffusion in the solid. *Acta Materialia*, 58(17):5749–5758, 2010.

14. A. Durga, P. Wollants, and N. Moelans. A quantitative phase-field model for two-phase elastically inhomogeneous systems. *Computational Materials Science*, 99:81–95, 2015.